Title

Fluorescence Correlation Spectroscopy Reveals Highly Efficient Cytosolic Delivery of Certain Penta-Arg Proteins and Stapled Peptides

Journal

Journal of the American Chemical Society, 137(7)

ISSN

0002-7863

Authors

LaRochelle, Jonathan R
Cobb, Garrett B
Steinauer, Angela
et al.

Publication Date

2015-02-25

DOI

10.1021/ja510391n

Peer reviewed

HHS Public Access

Author manuscript

J Am Chem Soc. Author manuscript; available in PMC 2016 January 05.

Published in final edited form as:

J Am Chem Soc. 2015 February 25; 137(7): 2536–2541. doi:10.1021/ja510391n.

Fluorescence Correlation Spectroscopy Reveals Highly Efficient Cytosolic Delivery of Certain Penta-Arg Proteins and Stapled Peptides

Jonathan R. LaRochelle[#§], **Garrett B. Cobb**[#‡], **Angela Steinauer**[†], **Elizabeth Rhoades**[*,‡], and **Alanna Schepartz**[*,†,§]

[†]Department of Chemistry, Yale University, New Haven, Connecticut 06520-8107, United States

[‡]Department of Molecular Biophysics and Biochemistry, Yale University, New Haven, Connecticut 06520-8107, United States

[§]Department of Molecular, Cellular and Developmental Biology, Yale University, New Haven, Connecticut 06520-8107, United States

[#] These authors contributed equally to this work.

Abstract

We used fluorescence correlation spectroscopy (FCS) to accurately and precisely determine the relative efficiencies with which three families of “cell-penetrating peptides” traffic to the cytosol of mammalian cells. We find that certain molecules containing a “penta-arg” motif reach the cytosol, intact, with efficiencies greater than 50%. This value is at least 10-fold higher than that observed for the widely studied cationic sequence derived from HIV Tat or polyarginine Arg_8, and equals that of hydrocarbon-stapled peptides that are active in cells and animals. Moreover, we show that the efficiency with which stapled peptides reach the cytosol, as determined by FCS, correlates directly with their efficacy in cell-based assays. We expect that these findings and the associated technology will aid the design of peptides, proteins, and peptide mimetics that predictably and efficiently reach the interior of mammalian cells.

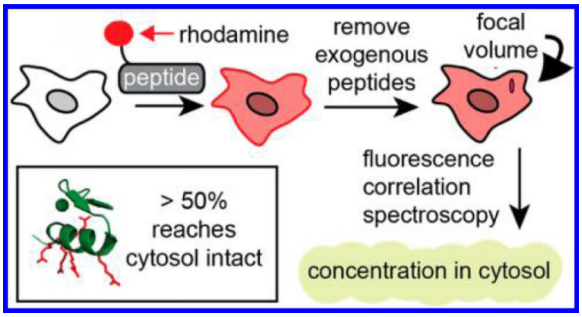

[*]**Corresponding Authors**alanna.schepartz@yale.edu, elizabeth.rhoades@yale.edu.

The authors declare no competing financial interest.

Supporting Information

Methods of peptide and Rho-peptide conjugate synthesis, confocal microscopy, fractionation, and supplementary figures and tables. This material is available free of charge via the Internet at http://pubs.acs.org.

INTRODUCTION

The discovery in 1988 that the HIV protein Tat could activate transcription when added intact to cultured cells[1,2] engendered a new scientific discipline focused on understanding how certain polar, positively charged, peptidic molecules cross nonpolar biological membranes.[7] Interest in the peptide translocation field has continued to grow, fueled in large part by an ever-increasing emphasis on biologicals, peptides, proteins, and their mimetics as tools in research and a growing segment of the modern pharmacopoeia. The chemistry of the peptide translocation process, that is, the role of cation identity and spacing, concentration, backbone, stereochemistry, appended cargo,[8–13] and the effect of endosomolytic agents,[13,14] have all been studied, as has the traffic pattern, which can include both endocytotic and nonendocytotic routes.[15,16]

Most studies of potentially cell-penetrating peptides and proteins employ either flow cytometry or a functional assay to evaluate uptake. Both techniques are inadequate, whether applied alone or in combination. Flow cytometry cannot differentiate molecules in the cytosol from those trapped in endosomes, and functional assays often amplify what is otherwise an undetectably small signal. Several groups have reported strategies to measure cytosolic localization using turn-on modules that fluoresce only in the reducing environment of the cytosol. Although these strategies recognize the need to assess cytosolic localization, and not total cell uptake, their output is both qualitative and indirect.[17–19]

Here we apply fluorescence correlation spectroscopy (FCS)[20] to accurately and precisely determine the cytosolic concentrations achieved by three families of potentially cell-penetrating peptides, and in this way directly establish their capacity to traffic to the cell interior. We find that certain molecules containing a “penta-arg” motif[16,21,22] reach the cytosol with efficiencies greater than 50%. This value is 10-fold higher than those observed for the widely studied sequence derived from HIV Tat[1–3] or Arg_8, and is comparable to the value achieved by hydrocarbon-stapled peptides that act in cells and animals.[5,6,23] Further, we demonstrate for a well-studied series that the potency of a hydrocarbon-stapled peptide in cell-based assays correlates directly with cytosolic localization as determined by FCS, and not by overall uptake as measured by flow cytometry.

In previous work, we reported that although many small folded proteins containing four to six arginines are taken up by cells,[21,22] very few traffic to the cytosol.[16] Those that do, such as ZF 5.3 and aPP 5.3 (referred to as 5.3 henceforth) (Figure 1B) are distinguished by a precise array of five arginines on an α-helix backbone, a “penta-arg” motif (Figure 1).[16] We showed further that proteins containing a penta-arg motif are taken up by endocytosis, and that a single penta-arg motif specifies release of the associated protein from vesicles that form early along the endosomal pathway, in particular, those endosomes characterized by the guanosine triphosphatase (GTPase) Rab5.[16] The role of early endocytic vesicles has also been implicated in the passage of supercharged proteins,[13] cyclic peptides,[24] and the contents of lipid nanoparticles[25] into the cell interior.

In previous work, we made use of an imaging assay called GIGT[16,26] to qualitatively evaluate the cytosolic access of penta-arg proteins as well as the cationic sequence from Tat

($Tat_{48–60}$) and Arg_8.[4] Although useful for comparing relative cytosolic access in high throughput across a large cell population, GIGT relies on dexamethasone-tagged molecules[27–30] and the translocation of a reporter protein (a fusion between GFP and a glucocorticoid receptor variant) from the cytosol to the nucleus as a proxy for cytosolic concentration. Although rapid, the GIGT assay is indirect and qualitative, as are other recently reported assays based on fluorescence dequenching in the cytosol.[17,19,31]

Here, we apply fluorescence correlation spectroscopy (FCS),[20] a quantitative technique with single molecule sensitivity, to provide a precise, accurate, and direct measure of the relative efficiencies with which different potentially cell-permeable molecules traffic to the cell interior.[32–35] FCS detects the fluctuations that arise when a small number of fluorescently tagged molecules diffuse through a small (in this case, ~1.6 femtoliter) focal volume.[20] The time-dependence of these fluctuations can be autocorrelated to determine both the diffusion dynamics and the concentration of the fluorophore-bearing molecule. FCS is unique as it does not rely on relative comparisons of fluorescence intensity but rather determines an absolute value for the intracellular fluorophore concentration. Although others have previously utilized FCS to measure cytoplasmic levels of the *Antennapedia* homeodomain-derived penetratin peptide and fibroblast growth factor-derived MTS peptide in adherent cells,[36,37] we were concerned by the high background signal observed and the pH-sensitivity and photoinstability of carboxyfluorescein conjugates, and developed an alternative FCS methodology.[38]

EXPERIMENTAL SECTION

Determination of Intracellular Concentrations Using FCS

One day prior to experiments, 20 000 HeLa cells in 400 μL of clear DMEM containing 10% FBS, 100 units/mL penicillin, and 100 μg/mL streptomycin were plated into 48-well tissue culture treated plates (Corning CLS3548) and allowed to adhere overnight. The following day, media was removed from each well and replaced with 250 μL of clear DMEM (no FBS or phenol red) containing the lissamine rhodamine b labeled peptide of interest (Rho-peptide) at a concentration of 500 nM. Cells were incubated with 500 nM Rho-peptide for 30 min at 37 °C, after which cells were washed three times with 1 mL of PBS and lifted with 100 μL of 0.25% trypsin for 3 min at 37 °C. The cells were next transferred into a 1.5 mL Eppendorf tube to which 1 mL of clear DMEM with 10% FBS was added, and were pelleted at 500*g* for 2 min. Following centrifugation, the media was removed and the cells were resuspended in 1 mL of clear DMEM (no FBS), pelleted at 300*g* for 2 min, resuspended in 200 μL of clear DMEM, and transferred to a Lab-Tek 8-chamber borosilicate coverglass system. Cells were allowed to adhere to the glass surface for 20 min at 37 °C prior to FCS measurements.

FCS Instrumentation

FCS measurements were made on a custom-built instrument based on an inverted Olympus IX-71 microscope, as described,[39,40] using a 60× water immersion objective (UPlanSApo, Olympus) at room temperature. Single cells were centered above the objective and imaged by stage scanning in the *x*–*z* dimensions using a piezoelectric Nano-LP200 nanopositioner

(Mad City Laboratories, Madison, WI). The positioner was controlled by custom programs written in LabView (National Instruments). Imaging scans revealed endosome-free locations suitable for FCS measurements.

FCS Setup

Laser power was adjusted to 10 μW prior to entering the microscope, and for Rho-peptide conjugates that emit less than 2000 counts per molecule (cpm) at 10 μW, a higher power of 30 μW was set. For Rho-b experiments, a 561 nm laser was used in combination with a 561 dichroic mirror and 605/70 bandpass filter. All filters and dichroics were from Chroma. The fluorescence emission was focused onto the aperture of a 50 μm diameter optical fiber (OzOptics) directly coupled to an avalanche photodiode (APD) for detection (SPCM-AQRH-14-FC; PerkinElmer). The signal from the APD was hardware correlated (Flex03LQ-12, Correlator.com).

Analysis of Correlation Functions

Autocorrelation curves from in vitro measurements were fit to a 3D diffusion equation (eq 1):

$$G(\tau) = \left(\frac{1}{N}\right) \frac{1}{\left(1+\frac{\tau}{\tau_{diff}}\right)\sqrt{\left(1+s^2\frac{\tau}{\tau_{diff}}\right)}} \quad (1)$$

N is average number of diffusing molecules in the observation volume, and τ_{diff} is the diffusion time, the average time a molecule takes to transit the laser focus. The structure factor, *s*, is the ratio of the radial to axial dimensions of the focal volume. *s* was determined to be 0.13 by measurement with Alexa 594 and fixed in subsequent analyses. Alexa 594 was routinely used to calibrate the instrument prior to measurements.

Correlation curves from intracellular peptides were initially fit to FCS equations incorporating multiple models of particle diffusion, including single component, multiple component, and anomalous diffusion. We found the data best fit to an equation describing anomalous diffusion (eq 2):

$$G(\tau) = \left(\frac{1}{N}\right) \frac{1}{\left(1+\frac{\tau}{\tau_{diff}}\right)^{\alpha}\sqrt{\left(1+s^2\frac{\tau}{\tau_{diff}}\right)^{\alpha}}} + G(\infty) \quad (2)$$

τ_{diff} represents the diffusion time and $G(\infty)$ represents the level of background autocorrelation at long time scales, while α represents the anomalous coefficient, which describes the extent to which diffusion is hindered over longer distances. Anomalous diffusion is often described in the cellular context, when barriers to diffusion include the presence of organelles and cytoskeleton.[41]

RESULTS AND DISCUSSION

We began by developing an FCS workflow to accurately and precisely determine the concentrations of rhodamine-peptide conjugates in vitro. The fluorescence spectrum of the

dye chosen, Rho-b, shows excitation and emission maxima at 566 and 585 nm respectively (Figure S1A, Supporting Information), which guided our choice of a 605/70 nm band-pass filter to maximize photon collection. The optimized FCS workflow yielded consistent in vitro Rho-b counts per molecule (cpm) around 10^4 Hz (Figure S1B). To determine the accuracy of this FCS setup for measuring concentration, we prepared and analyzed a set of Rho-b standard solutions at concentrations between 4 and 100 nM (Figure S1C). The average number of fluorescent species in the focal volume (N_{obs}) (Figure 1 and S1D), as determined by fitting the FCS curves, showed the expected linear relationship with dye concentration, and allowed us to determine a conversion factor between N_{obs} and the known concentration of the fluorescent species. Furthermore, the measured diffusion time (τ_D) of Rho-b was used to calculate a diffusion coefficient (D) of approximately 420 $\mu m^2\ s^{-1}$, in excellent agreement with values reported by others.[42] Each of the Rho-peptide conjugates evaluated using the FCS workflow also yielded consistent in vitro cpm and diffusion times (τ_D) that correspond to diffusion coefficients predicted by the Stokes–Einstein equation (Figure S2 and Table S1).

With these standards in place, we sought to evaluate the cytosolic concentrations attained by three families of “cell-penetrating” peptides studied previously using GIGT[26] and other assays.[43,44] Included in the analysis were molecules possessing an intact penta-arg motif (5.3^R and ZF 5.3^R)[16] along with variants lacking such a motif (4.2^R, 4.3^R, ZF^R, and ZF 4.3^R). Molecules lacking a a penta-arg motif trafficked less efficiently to the cytosol when evaluated using GIGT. The well-studied HIV $Tat_{48–60}$ sequence (Tat)[1] as well as octa-arginine Arg_8[4] were also studied. Flow cytometry experiments revealed that these molecules were taken up with varying efficiency by HeLa cells (Figure 2). Uptake was highest for ZF 5.3^R, lowest for Tat^R, ZF^R, and ZF 4.3^R, and intermediate for Arg_8^R, 4.2^R, and 5.3^R. The relative uptake of the rhodamine-tagged molecules studied here is identical to that of analogous fluorescein-tagged molecules reported previously.[16]

To prepare for FCS analysis (Figure 3), HeLa cells were incubated with a Rho-tagged molecule (500 nM) for 30 min and washed extensively with buffer and trypsin until no plasma membrane-associated fluorescence was observable by laser-scanning confocal microscopy (Figure S3). All treated cells showed extensive punctate fluorescence and, in some cases, clear evidence of fluorescence within the cytosol (Figure 3A and S3). Individual cells were then placed on a home-built confocal imaging system and scanned along the x–z-dimensions to identify locations for focal volume placement within the cytosol that avoided regions with high punctate signal. The individual traces were assessed and averaged as described in the Supporting Information; representative averaged curves are shown in Figure 3A. Many rhodamine-tagged peptides studied by others display anomalous diffusion when evaluated using FCS, an observation attributed to intracellular events that hinder macromolecule movement such as confinement, immobilization, and association.[45] On this basis, we fit the FCS data to an autocorrelation function containing a parameter for anomalous subdiffusion.[45] The diffusion times (τ_D) of Rho-peptide conjugates within the cytosol and thus the measured diffusion constants (D) were collectively 4 to 10-fold greater than values acquired in vitro (Table S2), in agreement with the range of cytoplasmic diffusion observed by others.[46] Low quality measurements, perhaps resulting from poor

focal volume placement, were discarded on the basis of an anomalous coefficient (a) < 0.5 (Figure 3A) or poor signal (cpm < 1000 Hz).[47] The N_{obs} determined from fits to the remaining measurements were averaged to yield mean intracellular concentration (Figure 3A).

The FCS data revealed that the molecules studied displayed wide variation in maximal autocorrelation signal (Figure 3A), indicating broad variation in the extent they reach the cytosol (Figure 3B,C). Although ZF 5.3^R, 5.3^R, 4.2^R, and Arg$_8^R$ are all taken up efficiently by HeLa cells as judged by flow cytometry (Figure 2A), only 4.2^R, 5.3^R, and ZF 5.3^R traffic efficiently to the cytosol (Figure 3B,C). In the case of cells treated with 500 nM 4.2^R, 5.3^R, or ZF 5.3^R, the intracellular concentrations measured by FCS are 256 ± 114 nM, 250 ± 90 nM, and 354 ± 40 nM, respectively, corresponding to cytosolic delivery efficiencies of 50, 51, and >70% for 4.2^R, 5.3^R, and ZF 5.3^R. By contrast, the cytosolic delivery efficiencies of 4.3^R, 5.2^R, and ZF^R, as well as Tat^R and Arg$_8^R$, are low. Although Arg$_8^R$ and 5.2^R were taken up well by HeLa cells, as judged by flow cytometry analysis of total cell fluorescence (Figure 2), FCS indicates that very little of either material reaches the cytosol (Figure 3B); the value for Tat^R is 2%. Overall, the efficiency with which a penta-arg protein (5.3 and ZF 5.3) reaches the cytosol is 25-fold greater than Tat^R (9.7 ± 2.0 nm) and 12-fold greater than Arg$_8^R$ (22 ± 5.7 nm), respectively (Figure 3C).[48]

In previous work, we made use of a streptolysin-based assay to probe whether ZF 5.3 and 5.3 trafficked to the cytosol in an intact form.[16] These studies revealed that only full-length ZF 5.3^R was extracted from the cell cytoplasm, while 5.3^R displayed evidence of digestion, potentially by cathepsins B and D. To complement those experiments, in this work we treated HeLa cells with each Rho-peptide conjugate for 30 min and fractionated the cytosol via homogenization followed by ultracentrifugation (Figure 4A).[49] The cytosolic fraction of HeLa cells treated with 1 μM ZF 5.3^R shows a single fluorescent peak by UPLC analysis that comigrates with authentic ZF 5.3^R (Figure 4B), whereas the cytosolic fraction of HeLa cells treated with 1 μM 5.3^R or 4.2^R shows multiple fluorescent species (Figure 4C and S4), indicating degradation, although the point at which degradation occurs cannot be known with certainty. Analysis of the peak intensities in comparison with standards (Figure S4) indicates that more than 70% of ZF 5.3^R is isolated in an intact form within the cell cytosol; the corresponding numbers for 5.3^R and 4.2^R are 12 and <5%, respectively. Importantly, the cytosolic trafficking efficiency of ZF 5.3^R, which does not degrade, is comparable whether determined by fractionation (63%) or FCS (73%), providing further evidence that ZF 5.3^R traffics into the cytosol as an intact polypeptide.

Hydrocarbon-stapled peptides are a family of well-studied peptide mimetics with demonstrated utility as tools and potential therapeutics.[5,6,50–53] Molecules possessing an all-hydrocarbon staple resist proteolytic degradation[54,55] and can exhibit robust function in cell-based assays and in animals.[5,23] Yet the physicochemical features necessary to predictably achieve high cytosolic concentration remain poorly understood, especially among stapled peptides possessing equivalent charge and in vitro potency.[5,51,52] To help illuminate these features, we applied FCS to quantify the cytosolic delivery efficiencies of a series of previously studied stapled peptide inhibitors of the HDM2–p53 interaction.[51] This series includes SAH-p53-4, which binds with high affinity to HDM2 in vitro but is not taken up

well by Jurkat T-cells (as judged by flow cytometry),[51] as well as SAH-p53-6 through -8, which bind HDM2 in vitro with comparable affinities (K_d values between 50 nM and 60 nM), possess the same overall charge (+1), and are taken up to a similar level by Jurkat T-cells as judged by FACS.[51] Despite the parity among these metrics, only SAH-p53-8 causes death of HDM2-addicted SJSA-1 cells in culture.[51]

To determine if the relative potencies of these molecules would correlate with cytosolic localization, we incubated HeLa cells with the rhodamine conjugates of SAH-p53-4, 6, 7, or 8 (500 nM) (Figure 5A) for 30 min and evaluated both whole-cell uptake (using flow cytometry, Figure 2B) and cytosolic localization (using FCS, Figure 5B,C). With respect to whole-cell uptake, the set of molecules followed the order SAH-p53-8^R > SAH-p53-7^R ~ SAH-p53-4^R > SAH-p53-6^R (Figure 2B,D), in agreement with the results of experiments in Jurkat cells reported previously.[51] By contrast, with respect to cytosolic localization, the set of molecules followed the order SAH-p53-8^R >> SAH-p53-6^R ~ SAH-p53-7^R > SAH-p53-4^R (Figure 5B,C). In this case, SAH-p53-8^R was clearly superior, with a trafficking efficiency that exceeded 50% after a 30 min incubation, and little evidence of degradation (Figure S4). The corresponding efficiencies for SAH-p53-7^R, SAH-p53-6^R, and SAH-p53-4^R were 21 ± 6%, 26 ± 4%, and 12 ± 2%, respectively (Figure 5B,C). Taken together, these results demonstrate that stapled peptide inhibitors of p53-hDM2 complexation, which possess equivalent overall charge and in vitro target affinities,[51] reach the cytosol with variable efficiencies. The most active peptide mimetic, SAH-p53-8, also displays the greatest cytosolic delivery. Interestingly, FCS analysis of the analogous “unstapled” peptides (which carry alkene-bearing side chains but are not macrocyclized) indicates that these molecules are internalized at intermediate levels, lower than SAH-p53-8^R but higher than SAH-p53-7^R, SAH-p53-6^R, and SAH-p53-4^R (Figure S5). These results complement and provide further resolution to a broad analysis of stapled peptide penetration reported recently.[56]

CONCLUSIONS

Over the past 20 years there has been a sustained interest in molecules able to cross biological membranes, passively by diffusion, or actively upon engagement of cell surface receptors or by endocytosis. Irrespective of mechanism, this process has been difficult to quantify in a manner that separates transport efficiency from the stability and activity of the transported molecule. Here we apply fluorescence correlation spectroscopy (FCS), a technique with single molecule sensitivity, to accurately and precisely quantify the intracellular transport efficiency of three families of potentially cell-penetrating peptides. Using FCS, we discovered that molecules containing a “penta-arg” motif reach the cytosol intact, with exceptionally high efficiencies, in certain cases exceeding 50%. The transport efficiency of the most efficient penta-arg molecule, ZF 5.3 is at least 10-fold higher than that observed for the widely studied cationic sequence derived from HIV Tat[1–3] or polyarginine[4] Arg_8, and equals that of hydrocarbon-stapled peptides that are active in cells and animals.[5,6] Moreover, we show that the efficiency with which hydrocarbon-stapled peptides reach the cytosol, as determined by FCS, correlates directly with their efficacy in cell-based assays. Further work will be necessary to determine the extent to which these conclusions apply to other cell types, other scaffolds, and other cargo.[57] Nonetheless, we hope that these findings

and the associated technology will aid the further design and analysis of peptides, proteins, and peptide mimetics that predictably and efficiently reach the interior of mammalian cells.

Supplementary Material

Refer to Web version on PubMed Central for supplementary material.

ACKNOWLEDGMENTS

This work was supported by US National Institutes of Health (NIH) grants R01 GM74756 and CA170741 to A.S. and the National Science Foundation Grant MCB 0919853 and a seed grant from the Beverly and Raymond Sackler Institute to E.R. J.R.L. and G.C. gratefully acknowledge support from an NIH-funded Chemistry Biology Interface Training Program (T32GM067543). Angela Steinauer is a Howard Hughes Medical Institute International Student Research fellow.

REFERENCES

1. Green M, Loewenstein PM. Cell. 1988; 55:1179. [PubMed: 2849509]
2. Frankel AD, Pabo CO. Cell. 1988; 55:1189. [PubMed: 2849510]
3. Vives E, Brodin P, Lebleu B. J. Biol. Chem. 1997; 272:16010. [PubMed: 9188504]
4. Mitchell DJ, Kim DT, Steinman L, Fathman CG, Rothbard JB. J. Pept. Res. 2000; 56:318. [PubMed: 11095185]
5. Walensky LD, Kung AL, Escher I, Malia TJ, Barbuto S, Wright RD, Wagner G, Verdine GL, Korsmeyer SJ. Science. 2004; 305:1466. [PubMed: 15353804]
6. Verdine, GL.; Hilinski, GJ. Methods in Enzymology: Protein Engineering for Therapeutics, Part B. Wittrup, KD.; Verdine, GL., editors. Vol. 503. Elsevier; Amsterdam: 2012. p. 3
7. Schwarze SR, Ho A, Vocero-Akbani A, Dowdy SF. Science. 1999; 285:1569. [PubMed: 10477521]
8. Zorko M, Langel U. Adv. Drug Delivery Rev. 2005; 57:529.
9. Sundlass NK, Raines RT. Biochemistry. 2011; 50:10293. [PubMed: 21980976]
10. van den Berg A, Dowdy SF. Curr. Opin. Biotechnol. 2011; 22:888. [PubMed: 21489777]
11. Jones AT, Sayers EJ. J. Controlled Release. 2012; 161:582.
12. Ellis GA, Palte MJ, Raines RT. J. Am. Chem. Soc. 2012; 134:3631. [PubMed: 22303837]
13. Thompson DB, Villasenor R, Dorr BM, Zerial M, Liu DR. Chem. Biol. 2012; 19:831. [PubMed: 22840771]
14. Erazo-Oliveras A, Najjar K, La Dayani L, Wang TY, Johnson GA, Pellois JP. Nat. Methods. 2014; 11:861. [PubMed: 24930129]
15. Stanzl EG, Trantow BM, Vargas JR, Wender PA. Acc. Chem. Res. 2013; 46:2944. [PubMed: 23697862]
16. Appelbaum JS, LaRochelle JR, Smith BA, Balkin DM, Holub JM, Schepartz A. Chem. Biol. 2012; 19:819. [PubMed: 22840770]
17. Lee YJ, Datta S, Pellois JP. J. Am. Chem. Soc. 2008; 130:2398. [PubMed: 18251482]
18. Cheung JC, Chiaw PK, Deber CM, Bear CE. J. Controlled Release. 2009; 137:2.
19. Li Y-C, Rodewald, Luo W, Hoppmann C, Wong, Ee T, Lebreton S, Safar P, Patek M, Wang L, Wertman KF, Wahl GM. Cell Rep. 2014; 9:1946. [PubMed: 25464845]
20. Vamosi, G.; Damjanovich, S.; Szollosi, J.; Vereb, G. Current Protocols in Cytometry. Wiley; New York: 2009. Chapter 2, Unit 2 15
21. Daniels DS, Schepartz A. J. Am. Chem. Soc. 2007; 129:14578. [PubMed: 17983240]
22. Smith BA, Daniels DS, Coplin AE, Jordan GE, McGregor LM, Schepartz A. J. Am. Chem. Soc. 2008; 130:2948. [PubMed: 18271592]
23. Bernal F, Wade M, Godes M, Davis TN, Whitehead DG, Kung AL, Wahl GM, Walensky LD. Cancer Cell. 2010; 18:411. [PubMed: 21075307]

24. Qian Z, LaRochelle JR, Jiang B, Lian W, Hard RL, Selner NG, Luechapanichkul R, Barrios AM, Pei D. Biochemistry. 2014; 53:4034. [PubMed: 24896852]
25. Gilleron J, Querbes W, Zeigerer A, Borodovsky A, Marsico G, Schubert U, Manygoats K, Seifert S, Andree C, Stoter M, Epstein-Barash H, Zhang LG, Koteliansky V, Fitzgerald K, Fava E, Bickle M, Kalaidzidis Y, Akinc A, Maier M, Zerial M. Nat. Biotechnol. 2013; 31:638. [PubMed: 23792630]
26. Holub JM, Larochelle JR, Appelbaum JS, Schepartz A. Biochemistry. 2013; 52:9036. [PubMed: 24256505]
27. Yu P, Liu B, Kodadek T. Nat. Biotechnol. 2005; 23:746. [PubMed: 15908941]
28. Kwon YU, Kodadek T. J. Am. Chem. Soc. 2007; 129:1508. [PubMed: 17283989]
29. Kwon YU, Kodadek T. Chem. Biol. 2007; 14:671. [PubMed: 17584614]
30. Yu P, Liu B, Kodadek T. Nat. Protoc. 2007; 2:23. [PubMed: 17401333]
31. Chao TY, Raines RT. Mol. BioSyst. 2013; 9:339. [PubMed: 23340874]
32. Magde D, Webb WW, Elson E. Phys. Rev. Lett. 1972; 29:705.
33. Elson EL, Magde D. Biopolymers. 1974; 13:1.
34. Magde D, Elson EL, Webb WW. Biopolymers. 1974; 13:29. [PubMed: 4818131]
35. Rigler R, Mets U, Widengren J, Kask P. Eur. Biophys. J. Biophys. Lett. 1993; 22:169.
36. Waizenegger T, Fischer R, Brock R. Biol. Chem. 2002; 383:291. [PubMed: 11934267]
37. Fischer R, Waizenegger T, Kohler K, Brock R. Biochim. Biophys. Acta. 2002; 1564:365. [PubMed: 12175919]
38. Hinkeldey B, Schmitt A, Jung G. ChemPhysChem. 2008; 9:2019. [PubMed: 18816535]
39. Elbaum-Garfinkle S, Rhoades E. J. Am. Chem. Soc. 2012; 134:16607. [PubMed: 22998648]
40. Trexler AJ, Rhoades E. Biochemistry. 2009; 48:2304. [PubMed: 19220042]
41. Weiss M, Hashimoto H, Nilsson T. Biophys. J. 2003; 84:4043. [PubMed: 12770908]
42. Culbertson CT, Jacobson SC, Michael Ramsey J. Talanta. 2002; 56:365. [PubMed: 18968508]
43. Choi YS, David AE. Curr. Pharm. Biotechnol. 2014; 15:192. [PubMed: 24938895]
44. Copolovici DM, Langel K, Eriste E, Langel U. ACS Nano. 2014; 8:1972. [PubMed: 24559246]
45. Wachsmuth M, Waldeck W, Langowski J. J. Mol. Biol. 2000; 298:677. [PubMed: 10788329]
46. Kuhn T, Ihalainen TO, Hyvaluoma J, Dross N, Willman SF, Langowski J, Vihinen-Ranta M, Timonen J. PLoS One. 2011; 6:e22962. [PubMed: 21886771]
47. Please see Supporting Information for additional details.
48. Interestingly, the GIGT assay yields high translocation ratios (TRs) for ZF 5.3^{Dex}, 5.3^{Dex}, Tat^{Dex} and Arg_8^{Dex}, while efficient delivery, as measured via FCS, was observed only for ZF 5.3^{R}, 4.2^{R} and 5.3^{R}. This discrepancy may be due to the greater affinities of TatDex and Arg8 Dex for the glucocorticoid receptor (GR) than 5.3^{Dex} or differential endocytic uptake, trafficking and/or release between dexamethasone and rhodamine peptide conjugates.
49. Aniento, F.; Gruenberg, J. Current Protocols in Immunology. Wiley; New York: 2003. Chapter 8, Unit 8 1C
50. Walensky LD, Pitter K, Morash J, Oh KJ, Barbuto S, Fisher J, Smith E, Verdine GL, Korsmeyer S. J. Mol. Cell. 2006; 24:199.
51. Bernal F, Tyler AF, Korsmeyer SJ, Walensky LD, Verdine GL. J. Am. Chem. Soc. 2007; 129:5298.
52. Moellering RE, Cornejo M, Davis TN, Del Bianco C, Aster JC, Blacklow SC, Kung AL, Gilliland DG, Verdine GL, Bradner JE. Nature. 2009; 462:182. [PubMed: 19907488]
53. Baek S, Kutchukian PS, Verdine GL, Huber R, Holak TA, Lee KW, Popowicz GM. J. Am. Chem. Soc. 2012; 134:103. [PubMed: 22148351]
54. Bird, GH.; Bernal, F.; Pitter, K.; Walensky, LD. Programmed Cell Death, the Biology and Therapeutic Implications of Cell Death, Part B. KhosraviFar, R.; Zakeri, Z.; Lockshin, RA.; Piacentini, M., editors. Vol. 446. Academic Press; Waltham, MA: 2008. p. 369
55. Schafmeister CE, Po J, Verdine GL. J. Am. Chem. Soc. 2000; 122:5891.
56. Chu Q, Moellering RE, Hilinski GJ, Kim Y-W, Grossmann TN, Yeh JT-H, Verdine GL. MedChemComm. 2015; 6:111–119.

57. Puckett CA, Barton JK. J. Am. Chem. Soc. 2009; 131:8738. [PubMed: 19505141]

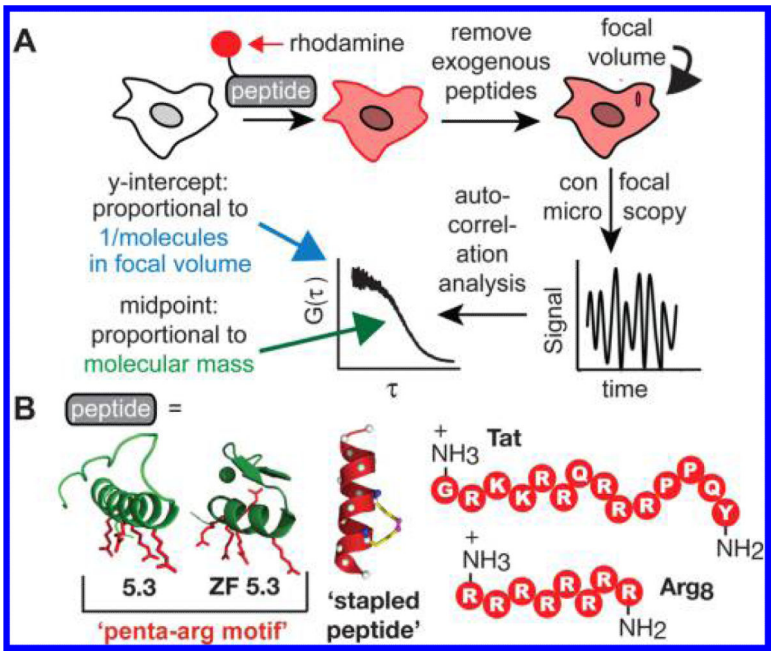

Figure 1.

(A) FCS workflow to determine the cytosolic concentration of a rhodamine-tagged molecule. (B) Three families of cell-penetrating molecules studied using FCS in this report.

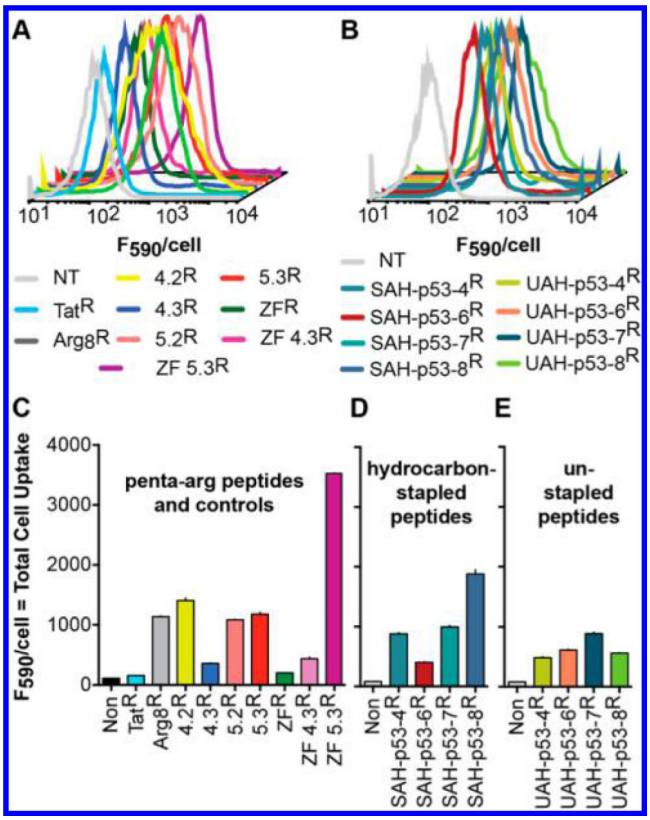

Figure 2.

Total cell uptake as measured by flow cytometry. (A, B) Flow cytometry histograms and (C–E) bar plots illustrating the relative uptake of the indicated Rho-tagged molecule (500 nM) after 30 min incubation with HeLa cells. Values of F_{590}/cell reflect the total cell-associated fluorescence, including fractions associated with the cell surface, endosomal compartments, as well as molecules that have reached the cytosol.

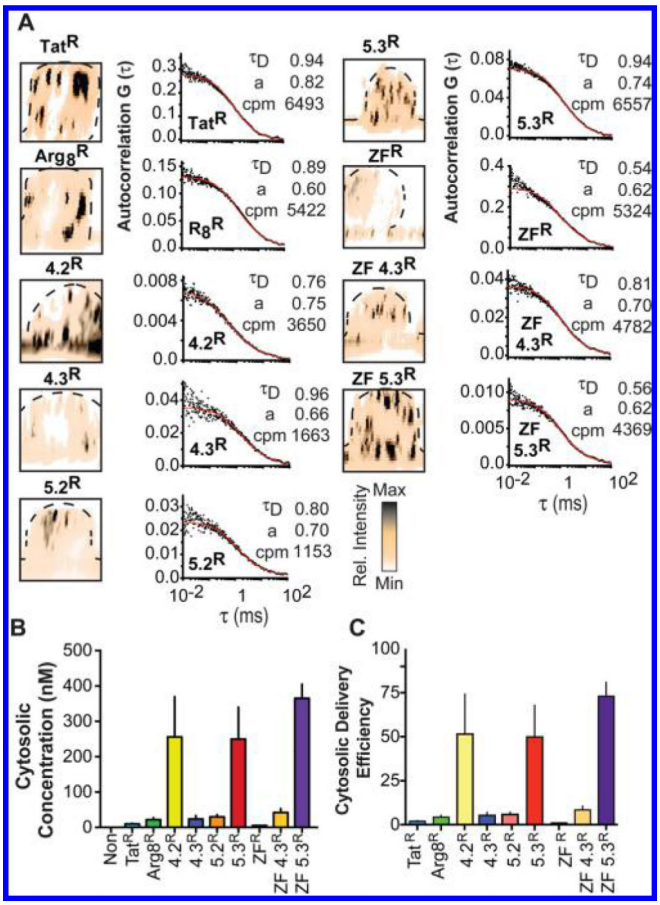

Figure 3.

Quantifying cytosolic delivery efficiencies of rhodamine-peptide conjugates using fluorescence correlation spectroscopy (FCS). (A) Representative *x*,*z*-section fluorescence intensity scans of single HeLa cells treated for 30 min with the indicated Rho-tagged peptide alongside the corresponding FCS trace displaying the diffusion time (τ_D), anomalous coefficient (a), and counts per molecule (cpm, Hz) associated with that individual measurement. Cell outlines are shown as dotted lines. (B) Intracellular concentrations of rhodamine-peptide conjugates extrapolated from respective autocorrelation fits. The value shown represents the average concentration of between 8 and 50 cells. (C) Cytosolic delivery efficiency of respective rhodamine-peptide conjugates determined by dividing the intracellular concentration by treatment concentration. Error bars represent standard error of the mean.

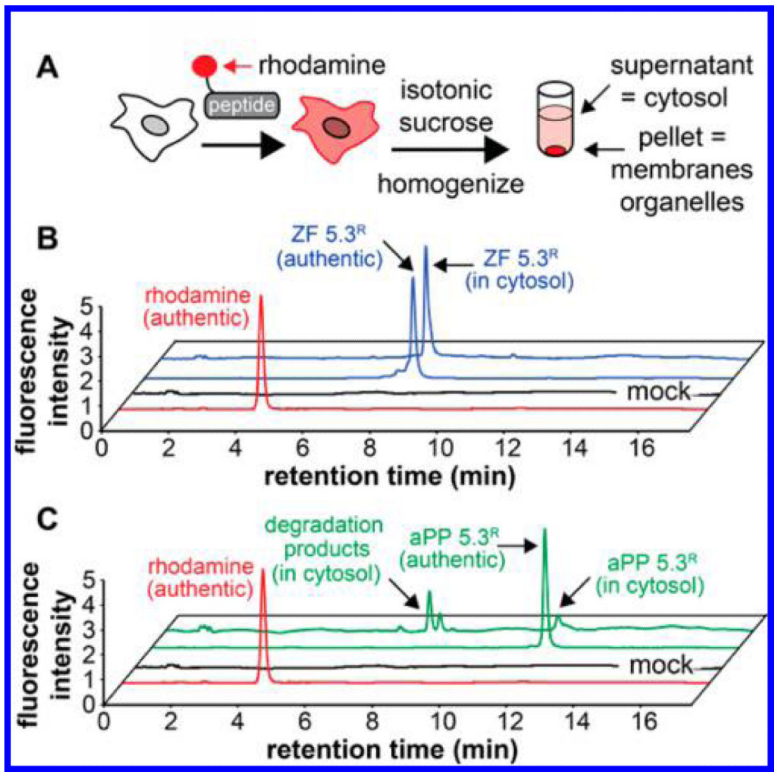

Figure 4.

Biochemical analysis of HeLa cell cytosol after incubation with ZF 5.3^{R} and 5.3^{R}. (A) HeLa cells were treated with 1 μM of either ZF 5.3^{R} and 5.3^{R} for 30 min before homogenization in an isotonic sucrose solution and ultracentrifugation at 100*g* for 30 min. (B, C) Samples of the supernatant after ultracentrifugation were injected onto a Shimadzu UFLC-XR UPLC alongside authentic samples and resolved on an Agilent Poroshell 120 SB-C18 column at 580 nm.

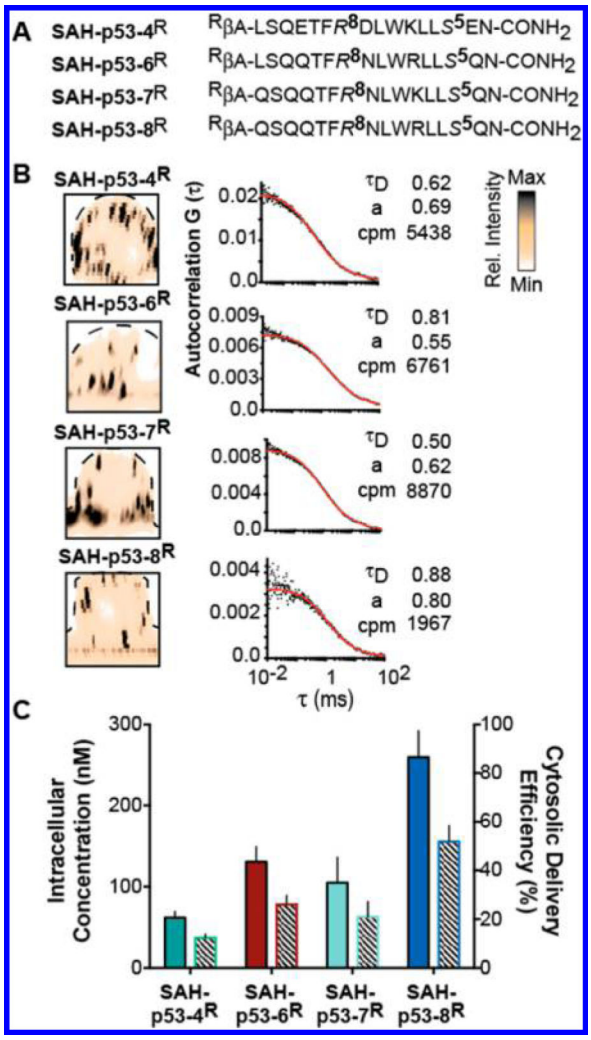

Figure 5.

FCS analysis of intracellular concentrations achieved in HeLa cells by hydrocarbon-stapled peptide inhibitors of p53-HDM2 complexation. (A) Sequences of hydrocarbon-stapled peptides analyzed herein. (B) Representative *x*,*z*-section fluorescence intensity scans of single HeLa cells treated for 30 min with the indicated Rho-tagged molecule under standard culture conditions, and corresponding intracellular FCS traces displaying diffusion time (τ_D), anomalous coefficient (*a*), and counts per molecule (cpm, Hz) values. Cell outlines are shown as dotted lines. (C) Intracellular concentrations of Rho-tagged molecules extrapolated from respective autocorrelation fits (solid bars) and corresponding cytosolic delivery efficiencies (hatched bars). Error bars represent standard error of the mean.